

# Iron Isotope Fractionation during Fe(II) Oxidation Mediated by the Oxygen-Producing Marine Cyanobacterium *Synechococcus* PCC 7002

E. D. Swanner,<sup>\*,†</sup> T. Bayer,<sup>‡</sup> W. Wu,<sup>‡</sup> L. Hao,<sup>‡,#</sup> M. Obst,<sup>§</sup> A. Sundman,<sup>‡</sup> J. M. Byrne,<sup>‡</sup> F. M. Michel,<sup>||</sup> I. C. Kleinhanns,<sup>‡</sup> A. Kappler,<sup>‡</sup> and R. Schoenberg<sup>‡</sup>

<sup>†</sup>Iowa State University, Department of Geological & Atmospheric Sciences, 2237 Osborn Drive, 253 Science I, Ames, Iowa 50011-1027, United States

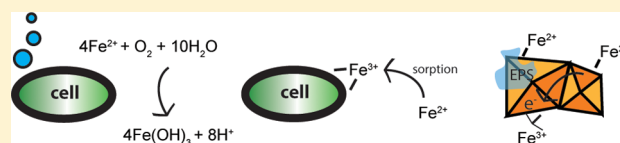
<sup>‡</sup>University of Tuebingen, Department of Geosciences, Tuebingen, Germany

<sup>§</sup>University of Bayreuth, Bayreuth Center of Ecology and Environmental Research, Dr-Hans-Frisch-Str. 1-3, 95448 Bayreuth, Germany

<sup>||</sup>Department of Geosciences, Virginia Tech, Blacksburg, Virginia 24061-0420, United States

## S Supporting Information

**ABSTRACT:** In this study, we couple iron isotope analysis to microscopic and mineralogical investigation of iron speciation during circumneutral Fe(II) oxidation and Fe(III) precipitation with photosynthetically produced oxygen. In the presence of the cyanobacterium *Synechococcus* PCC 7002, aqueous Fe(II) (Fe(II)<sub>aq</sub>) is oxidized and precipitated as amorphous Fe(III) oxyhydroxide minerals (iron precipitates, Fe<sub>ppt</sub>), with distinct isotopic fractionation ( $\epsilon^{56}\text{Fe}$ ) values determined from fitting the  $\delta^{56}\text{Fe}(\text{II})_{\text{aq}}$  (1.79‰ and 2.15‰) and the  $\delta^{56}\text{Fe}_{\text{ppt}}$  (2.44‰ and 2.98‰) data trends from two replicate experiments. Additional Fe(II) and Fe(III) phases were detected using microscopy and chemical extractions and likely represent Fe(II) and Fe(III) sorbed to minerals and cells. The iron desorbed with sodium acetate (Fe<sub>NaAc</sub>) yielded heavier  $\delta^{56}\text{Fe}$  compositions than Fe(II)<sub>aq</sub>. Modeling of the fractionation during Fe(III) sorption to cells and Fe(II) sorption to Fe<sub>ppt</sub> combined with equilibration of sorbed iron and with Fe(II)<sub>aq</sub> using published fractionation factors, is consistent with our resulting  $\delta^{56}\text{Fe}_{\text{NaAc}}$ . The  $\delta^{56}\text{Fe}_{\text{ppt}}$  data trend is inconsistent with complete equilibrium exchange with Fe(II)<sub>aq</sub>. Because of this and our detection of microbially excreted organics (e.g., exopolysaccharides) coating Fe<sub>ppt</sub> in our microscopic analysis, we suggest that electron and atom exchange is partially suppressed in this system by biologically produced organics. These results indicate that cyanobacteria influence the fate and composition of iron in sunlit environments via their role in Fe(II) oxidation through O<sub>2</sub> production, the capacity of their cell surfaces to sorb iron, and the interaction of secreted organics with Fe(III) minerals.



## INTRODUCTION

Fe(II)-oxidizing bacteria (FeOB) gain energy from the chemical oxidation of Fe(II) coupled to reduction of oxygen or nitrate or using light energy coupled to reduction of CO<sub>2</sub>, e.g., anoxygenic photosynthesis.<sup>1</sup> At the near neutral pH of many surface waters, the oxidation of Fe(II) is spontaneous and rapid in the presence of dissolved oxygen. For that reason, cyanobacteria, which generate oxygen as a result of oxygenic photosynthesis, can act as indirect Fe(II)-oxidizing bacteria where anoxic and Fe(II)-containing waters encounter to sunlit surface environments.

The contribution of cyanobacteria to Fe(II) oxidation has been quantitatively addressed in Fe(II)-rich hot spring environments<sup>2</sup> and in benthic photosynthetic communities living at the sediment–water interface.<sup>3</sup> Although the modern oceans are predominantly oxygenated to great depths, promoting the speciation of iron as ferric [Fe(III)] rather than ferrous [Fe(II)], Fe(II) may be increasingly mobilized out of sediments<sup>4–7</sup> and stabilized in the marine water column due to expanding low-oxygen conditions in so-called oxygen minimum zones (OMZ).<sup>8</sup> Where OMZ intersect with the

photic zone, Fe(II) oxidation by planktonic oxygen-producing cyanobacteria could contribute to the marine iron cycle. Furthermore, anoxic and Fe(II)-rich bottom waters are a pervasive feature of oceans in the Precambrian Era [before about 500 Million years (My) ago]<sup>9,10</sup> at a time when oxygen was building up in the surface oceans as a result of cyanobacteria and other oxygenic phototrophs.<sup>11–13</sup> Therefore, redox interfaces between anoxic and Fe(II)-containing waters and photosynthetically produced oxygen were likely common throughout much of Earth's history.

Iron redox processes fractionate the naturally occurring isotopes of iron dependent on their mass (e.g., <sup>54</sup>Fe, <sup>56</sup>Fe, <sup>57</sup>Fe, and <sup>58</sup>Fe), such that the quantitative contribution of biotic and abiotic iron cycling at the Earth's surface may be recorded in sediments composed of iron-rich minerals.<sup>14,15</sup> Due to the large fractionations between Fe(II) and Fe(III) species,<sup>16</sup> Fe(II)

Received: November 18, 2016

Revised: April 10, 2017

Accepted: April 12, 2017

Published: April 12, 2017

oxidation generally produces a solid iron phase that is enriched in heavy isotopes of iron relative to aqueous Fe(II), regardless of the mechanism of oxidation.<sup>17</sup> This makes it difficult to parse the contribution of enzymatic Fe(II)-oxidizing bacteria from abiotic Fe(II) oxidation, not to mention indirect Fe(II) oxidation by oxygen-producing cyanobacteria by using iron isotopes. However, subtle differences in the mechanism of oxidation and precipitation, and in the characteristics of the iron minerals or phases (e.g., mineralogy, particle size, or presence of impurities) formed, can influence the overall fractionation between aqueous Fe(II) and iron minerals.<sup>18</sup> Furthermore, the role of cyanobacteria in direct or indirect redox cycling of iron at the cell surface is increasingly recognized<sup>19–22</sup> and may be associated with distinct isotope fractionation.<sup>23</sup> Therefore, detailed mechanistic studies of iron isotope fractionation during different pathways of Fe(II) oxidation are warranted and may help to define isotopic, mineralogical, or microscopic signatures associated with certain biological processes.

Furthermore, the isotopic composition of iron minerals is known to be modified by electron and atom exchange between aqueous Fe(II) and Fe(III) (oxyhydr)oxide minerals.<sup>24–26</sup> These processes have been most effectively characterized under reducing conditions, when a supply of aqueous Fe(II) is produced by, for instance, microbial Fe(III) reduction.<sup>27,28</sup> However, at Fe(II)–O<sub>2</sub> interfaces with a flux of aqueous Fe(II), electron and atom-exchange could also occur on newly formed Fe(III) (oxyhydr)oxide minerals.<sup>29</sup> Although the effect of some organics as well as Si and low pH on blocking electron and atom exchange have been investigated,<sup>30–32</sup> the effect of cell surfaces and microbially produced organics on this reaction and via blocking sites on Fe(III) minerals, particularly in an oxidizing system, are not known.

In this contribution, we tracked the iron isotope composition of different pools of iron during Fe(II) oxidation by the marine planktonic cyanobacterium *Synechococcus* PCC 7002. Several prior studies have characterized the interaction of this oxygen-producing strain with Fe(II),<sup>33,34</sup> which gives us a body of work to aid in interpreting the nature of different iron phases in the system, and their mechanism of transformation. Additional microscopy and mineral characterization in this study are used to build the picture of how iron is processed during indirect Fe(II) oxidation resulting from oxygenic photosynthesis. The results have implications for understanding the reactivity of iron minerals as well as identifying isotopic signatures associated with biological activity.

## ■ EXPERIMENTAL SECTION

**Bacterial Growth Medium.** *Synechococcus* PCC 7002 was routinely cultivated on pH 6.8 Marine Phototroph (MP) medium<sup>18,33,35</sup> containing 6 mg L<sup>-1</sup> ferric ammonium citrate as the Fe(III) source at 24 °C under an irradiance of 12.8 μmol photons m<sup>-1</sup> s<sup>-1</sup> from a standard 40W tungsten light bulb as measured by a Li-250A light probe (Li-cor, Inc.). For Fe(II) oxidation experiments, MP medium was made without ferric ammonium citrate. Fe(II) amendments were added from a sterile, anoxic FeCl<sub>2</sub> stock solution, and the medium was filtered twice through a 0.22 μm filter in an anoxic glovebox (100% N<sub>2</sub>), separated by 48 h incubations at 4 °C to ensure that all Fe(II) precipitated as carbonate and phosphate minerals with growth media components were removed.<sup>18</sup> The final Fe(II) concentration in the medium after filtration was 2 mM as measured by the spectrophotometric Ferrozine assay. A log-

phase culture of *Synechococcus* PCC 7002 grown with ferric ammonium citrate was degassed for 5 min with sterile N<sub>2</sub>/CO<sub>2</sub> (90%:10%) and inoculated into the 2 mM Fe(II)-containing medium to a final concentration of 5 × 10<sup>6</sup> cells mL<sup>-1</sup>.<sup>33</sup> Growth conditions were as above.

Glass media bottles were acid washed in 1 M HCl for 24 h and then soaked in fresh ultrapure water (resistivity of 18.2 MΩ cm<sup>-1</sup>) for two successive 24 h treatments before use. Experiments utilized 100 mL bottles filled to 80 mL with growth medium. All anoxic bottles were closed with butyl rubber stoppers that had been washed in 1 N HCl for 24 h and then thrice boiled in ultrapure water.

This concentration of 2 mM Fe(II) was chosen for experiments because a freshly inoculated culture of *Synechococcus* PCC 7002 took about 10 days to oxidize this, during which time we could sample sufficiently often to have resolution on the evolution of the isotopic composition of different iron pools. Despite the fact that this strain grows more slowly at 2 mM Fe(II) than at lower Fe(II) concentrations, due to Fe(II) toxicity,<sup>33,34</sup> sufficient growth did occur to fully oxidize all Fe(II). Although this concentration is at the upper end of Fe(II) concentrations in modern sunlit environments,<sup>36,37</sup> it is within the range documented for environments where cyanobacteria have been documented as having a role in Fe(II) oxidation.<sup>2,3</sup>

**Iron Species Separation and Fe(II) and Total Iron Concentration Determination.** During Fe(II) oxidation, which lasted about 10 days, volumes of 2 mL were repeatedly removed with a syringe from the bottles of two contemporaneous replicate experiments (bottles 1 and 2) in an anoxic glovebox. Before extracting, the bottles were shaken to yield a homogeneous slurry of iron precipitates. The aliquots were subsequently centrifuged for 10 min at 16 000g, and the supernatants were filtered through a nylon 0.22 μm centrifuge tube filter (Costar Spin-X, Corning, International) to yield particle-free aqueous Fe(II), henceforth Fe(II)<sub>aq</sub>. The solids were washed with anoxic ultrapure water to remove any loosely bound iron. A second wash utilized anoxic 0.5 M sodium acetate (adjusted to pH 4.85 using acetic acid) to recover sorbed iron (Fe<sub>NaAc</sub>) from the solids (24 h incubation in the dark).<sup>29,38</sup> The remaining solids were considered the precipitated fraction (Fe<sub>ppt</sub>).

The concentrations of Fe(II) and total iron in the four different iron fractions were measured with the ferrozine assay.<sup>39</sup> The Fe(II) in the Fe(II)<sub>aq</sub> water wash, and Fe<sub>NaAc</sub> was stabilized in a final concentration of anoxic 1 M HCl prior to measurements. The Fe<sub>ppt</sub> was dissolved in anoxic 6 N HCl before analysis. Fe(III) was determined as the difference between Fe(II) measurement and total iron measurements (after reduction of iron by hydroxylamine hydrochloride).

**Fe Isotope Analysis.** Purification of the Fe(II)<sub>aq</sub>, Fe<sub>NaAc</sub>, and Fe<sub>ppt</sub> fractions was performed in positively pressured clean laboratories of the Isotope Geochemistry group at the University of Tuebingen under conditions and with reagents that have previously been described.<sup>40</sup> The concentrations of iron in the water washes of Fe<sub>ppt</sub> were below the detection limit of the ferrozine assay (<0.01 mM, 0.56 μg mL<sup>-1</sup>), and so, these samples were not purified. Sample aliquots of the separated iron fractions containing 5 μg of iron were purified for iron isotope measurements using anion exchange chromatography according to prior methodology.<sup>40</sup> An adequate amount of <sup>57</sup>Fe–<sup>58</sup>Fe double spike was added to the samples prior to Fe purification to ensure accurate correction of the instrumental

Table 1. Iron Isotope Data from Experiments with *Synechococcus* PCC 7002<sup>a</sup>

replicate	sample	fraction of Fe(II) oxidized	$\delta^{56}\text{Fe}_{\text{aq}}$ (‰)	2SE <sup>c</sup>	$\delta^{56}\text{Fe}_{\text{ppt}}$ (‰)	2SE <sup>c</sup>	$\delta^{56}\text{Fe}_{\text{NaAc}}$ (‰)	2SE <sup>c</sup>	
bottle 1	A1	0.00	0.13	0.05	ND		ND		
	B1	0.42	-0.34	0.03	ND		0.10	0.08	
	D1	0.36	-0.97	0.04	2.16	0.04	ND		
	E1	0.43	-1.22	0.04	1.96	0.03	-0.36	0.04	
	F1	0.49	-1.49	0.04	1.87	0.04	-0.65	0.04	
	G1	0.57	-1.75	0.05	1.74	0.03	ND		
	H1	0.60	-2.05	0.04	1.55	0.03	-0.42	0.05	
	I1	0.72	-2.53	0.05	1.25	0.03	-0.73	0.04	
	J1	0.81	-3.25	0.05	0.97	0.04	-0.59	0.04	
	K1	0.99	ND		0.10	0.04	ND		
	Rayleigh fit		$\epsilon^{56}\text{Fe}$	2.15		2.44		NA	
		$\Sigma\chi^2$	0.66		0.06				
linear fit		$\epsilon^{56}\text{Fe}$	2.90		3.42		NA		
		$\Sigma\chi^2$	0.85		0.38				
bottle 2	A2	0	-0.08	0.04	ND		ND		
	B2	0.47	-0.57	0.05	ND		-11.11 <sup>b</sup>	0.06	
	D2	0.41	-1.08	0.04	2.07	0.04	-0.33	0.06	
	E2	0.48	-8.75 <sup>b</sup>	0.07	1.97	0.03	-0.31	0.04	
	G2	0.57	-1.59	0.04	1.83	0.04	-0.18	0.04	
	H2	0.56	-1.75	0.05	1.75	0.04	-0.09	0.04	
	I2	0.65	-1.96	0.04	1.59	0.03	-0.57	0.04	
	J2	0.63	-2.04	0.04	1.58	0.04	ND		
	K2	0.99	ND		0.07	0.03	ND		
	Rayleigh fit		$\epsilon^{56}\text{Fe}$	1.79		2.98		NA	
			$\Sigma\chi^2$	0.47		0.36			
linear fit		$\epsilon^{56}\text{Fe}$	2.66		4.17		NA		
		$\Sigma\chi^2$	0.84		1.23				

<sup>a</sup>Each sample was measured twice. ND = not determined, due to a low amount of sample. NA = not applicable. <sup>b</sup>Samples from B2 and E2 had anomalous values for  $\delta^{56}\text{Fe}_{\text{NaAc}}$  and  $\delta^{56}\text{Fe}_{\text{aq}}$ , respectively. These samples were most likely lost after drying due to electrostatic charging of the Teflon beakers. These results are therefore excluded from further analysis. <sup>c</sup>SE refers to standard error.

mass bias and possible Fe isotope fractionation during anion chromatography caused by the organic matrix of the samples.<sup>18</sup> Iron isotope analyses were performed on the ThermoFisher Scientific NeptunePlus multicollector inductively coupled plasma mass spectrometer (MC-ICP-MS) of the Isotope Geochemistry group of the University of Tuebingen. Polyatomic interferences, such as  $^{40}\text{Ar}^{14}\text{N}^+$  on  $^{54}\text{Fe}^+$  or  $^{40}\text{Ar}^{16}\text{O}^+$  on  $^{56}\text{Fe}^+$  were resolved using the high mass-resolution mode (16  $\mu\text{m}$  slit). The four iron isotope beams were simultaneously detected with 90 integration cycles at 8 s each during the runs. Background corrections for sample signals were based on on-peak-zero measurements on the pure analyte solution (0.3 M  $\text{HNO}_3$ ) run before and after each sample. Iron isotope data are reported relative to the isotopically certified international reference material IRMM-014 (Institute for Reference Materials and Measurements in Gent, Belgium) using the  $\delta$ -notation:

$$\delta^{56}\text{Fe} = [({}^{56}\text{Fe}/{}^{54}\text{Fe})_{\text{sample}} / ({}^{56}\text{Fe}/{}^{54}\text{Fe})_{\text{IRMM-014}} - 1] \times 1000$$

The results are reported in units of per mil (‰). The reproducibility of the double-spike measuring method as determined by repeated  $\delta^{56}\text{Fe}$  measurements of the IRMM-014 reference material in between sample runs was  $0.00\text{‰} \pm 0.032\text{‰}$  (2SD;  $n = 18$ ). Interspersed measurements of our in-house iron standard, HanFe, yielded  $\delta^{56}\text{Fe} = 0.282\text{‰} \pm 0.039\text{‰}$  (2SD;  $n = 12$ ), which is in excellent agreement with previously published values of  $0.28\text{‰} \pm 0.05\text{‰}$  (2SD;  $n = 19$ )<sup>41</sup> and  $0.279\text{‰} \pm 0.030\text{‰}$  (2SD;  $n = 5$ ).<sup>18</sup>

Rayleigh fits of the isotopic  $\delta^{56}\text{Fe}(\text{II})_{\text{aq}}$  and  $\delta^{56}\text{Fe}_{\text{ppt}}$  at different fractions ( $f$ ) of Fe(II) remaining were utilized to determine the isotopic enrichment factor ( $\alpha^{56}\text{Fe}$ ) using the following equations:

$$\delta^{56}\text{Fe}(\text{II})_{\text{aq}} = (\delta^{56}\text{Fe}(\text{II})_{\text{aq-0}} + 1000) \times f^{\alpha-1} - 1000 \quad (1)$$

$$\delta^{56}\text{Fe}_{\text{ppt}} = (\delta^{56}\text{Fe}_{\text{aq-0}} + 1000) \times [(1 - f^{\alpha}) / (1 - f)] - 1000 \quad (2)$$

$\delta^{56}\text{Fe}(\text{II})_{\text{aq-0}}$  indicates the  $\delta^{56}\text{Fe}(\text{II})_{\text{aq}}$  at the beginning of the experiment. The isotopic fractionation  $\epsilon^{56}\text{Fe}$  (‰) is related to  $\alpha^{56}\text{Fe}$  by the equation:

$$\epsilon^{56}\text{Fe} = 1000 \times \ln \alpha^{56}\text{Fe} \quad (3)$$

The fitting parameters were determined by minimizing the sum of  $\chi^2$  values. Data were also fit by linear regression, with slope and intercept determined by minimizing the sum of  $\chi^2$  values.

**Mineral Characterization.** High energy synchrotron X-ray scattering experiments were performed on the solid, dry products of Fe(II) oxidation by *Synechococcus* PCC 7002 at the Advanced Photon Source at Argonne National Laboratory, Beamline 11-ID-B. The solids were collected from a culture grown with ca. 5 mM Fe(II), freeze-dried, and washed three times with Millipore water to remove excess salt. Data collection and analysis protocols were previously described.<sup>18</sup> Additional mineral characterization methods and results are described in the [Supporting Information](#).

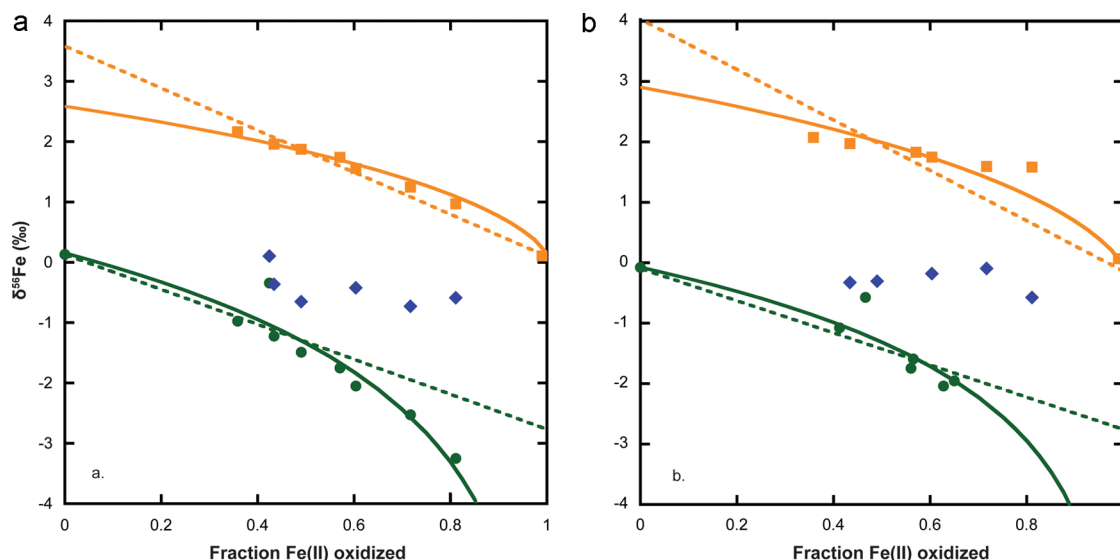


**Figure 1.** (a) Bottle 1 and (b) bottle 2 are biological replicates of the Fe(II) oxidation experiment with *Synechococcus* PCC 7002. Green circles are  $\delta^{56}\text{Fe}(\text{II})_{\text{aq}}$  data; orange squares are  $\delta^{56}\text{Fe}_{\text{ppt}}$  data; blue diamonds are  $\delta^{56}\text{Fe}_{\text{NaAc}}$  data. The solid green lines are the Rayleigh fits of the  $\delta^{56}\text{Fe}(\text{II})_{\text{aq}}$  data, with an  $\epsilon^{56}\text{Fe}$  for  $\text{Fe}(\text{II})_{\text{aq}}$  of 1.79‰ (a) to 2.15‰ (b). The solid orange lines are the Rayleigh fits of the  $\delta^{56}\text{Fe}_{\text{ppt}}$  data, with  $\epsilon^{56}\text{Fe}$  for  $\delta^{56}\text{Fe}_{\text{ppt}}$  of 2.44‰ (a) and 2.98‰ (b). The linear fits are shown as dotted lines for reference.

**Confocal Laser Scanning Microscopy.** Cells of *Synechococcus* PCC 7002 were grown under similar conditions as described above until the initial ca. 4.5 mM Fe(II) had been oxidized. The cell–mineral aggregates were imaged by confocal laser scanning microscopy (CLSM; Leica SPE, Mannheim, Germany). A 635 nm laser was used for excitation autofluorescence of *Synechococcus* PCC 7002, with a maximum emission peak at 660 nm (detected range of emission, 640–700 nm). The Fe(III) minerals were visualized using the reflection signal of the 488 nm laser. Several lectin–Alexa dye conjugates were screened in order to optimize visualization of exopolysaccharides (EPS) without overlap with the autofluorescence emission maximum of the pigments of *Synechococcus* PCC 7002 (660 nm). SBA–Alexa 488 (maximum emission peak at 520 nm) was chosen because SBA bound to the EPS in higher amounts, resulting in brighter fluorescence than the other lectins screened [Wheat Germ Agglutinin Alexa Fluor 555 Conjugate (WGA-555) and Lectin PNA from *Arachis hypogaea* (peanut), Alex Fluor 568 Conjugate (PNA-568)]. Brighter fluorescence at lower laser power was observed with SBA-488, which binds terminal  $\alpha$ - and  $\beta$ -*N*-acetylgalactosamine and galactopyranosyl residues, compared to WGA-555 and PNA-568, which are specific to sialic acid and *N*-acetylglucosaminyl residues and terminal  $\beta$ -galactose, respectively.

A turn-on type selective probe for fluorescent labeling of dissolved, sorbed, or ligand-bound Fe(III)<sup>42,43</sup> was previously used to visualize the relationship of Fe(III) *Synechococcus* PCC 7002 cells and minerals from this same incubation.<sup>34</sup> Because of spectral overlap, the lectin and Fe(III)-binding probe could not be combined in a single experiment here, and therefore, we compare new results to prior data.<sup>34</sup> The Auto-Quant deconvolution algorithm implemented in the LEICA LAS AF software was applied to blind deconvolute the 3D image stacks.<sup>44</sup> The spatial relationships of species detected using fluorescence dyes and cell autofluorescence in CLSM image stacks were analyzed using ScatterJ,<sup>45</sup> a plugin for correlation analysis of species-specific maps for use in IMAGEJ and Fiji.<sup>46</sup>

## RESULTS AND DISCUSSION

**Fractionation Patterns during Fe(II) Oxidation and Fe(III) Precipitation.** The  $\delta^{56}\text{Fe}(\text{II})_{\text{aq}}$  values from two replicated experiments evolved from an initial value near 0‰ to lighter values during oxidation (Table 1, Figure 1). The  $\text{Fe}(\text{II})_{\text{aq}}$  fraction, measured after the sample was centrifuged and filtered, consisted of only Fe(II). All iron concentration and speciation data (measured by ferrozine) is reported in Supplementary Table 1. The first  $\text{Fe}_{\text{ppt}}$  samples analyzed, at about 40% Fe(II) oxidized, had  $\delta^{56}\text{Fe}_{\text{ppt}}$  of about 2‰, trending toward 0‰ at 100% Fe(II) oxidized. The speciation of  $\text{Fe}_{\text{ppt}}$ , which was measured after washing with water and sodium acetate, consisted of predominantly Fe(III), with generally <10% Fe(II). Iron in the water wash of the precipitates was below the detection limit of the ferrozine assay (<0.01 mM,  $0.56 \mu\text{g mL}^{-1}$ ). Therefore, the iron isotope composition of the water washes was not analyzed. The sodium acetate wash removed sorbed iron, which contained both Fe(II) and Fe(III). The  $\text{Fe}_{\text{NaAc}}$  fraction represented 10–20% of total iron in the system after  $\text{Fe}_{\text{ppt}}$  began to form. The  $\text{Fe}_{\text{NaAc}}$  had an intermediate isotopic composition between  $\text{Fe}(\text{II})_{\text{aq}}$  and  $\text{Fe}_{\text{ppt}}$  but was variable and generally lighter than 0‰.

The fast reaction between Fe(II) and oxygen<sup>47</sup> favors the heavy isotopes of iron in the resulting Fe(III) minerals that precipitate. Abiotic and biotic Fe(II) oxidation both follow this trend, resulting in  $\epsilon^{56}\text{Fe}$  of  $\sim 2$ – $4$ ‰ between aqueous Fe(II) and Fe(III) minerals, with minerals enriched in heavy isotopes.<sup>17,18,29,31</sup> Our  $\epsilon^{56}\text{Fe}$  for  $\delta^{56}\text{Fe}(\text{II})_{\text{aq}}$  (1.79–2.15‰ for bottles 1 and 2, respectively; Table 1), determined from a Rayleigh fit of the  $\delta^{56}\text{Fe}(\text{II})_{\text{aq}}$  data, is on the low end of this range, similar to what was previously documented for Fe(II) oxidation by anoxygenic phototrophs.<sup>18,48</sup> The Rayleigh fit of the  $\delta^{56}\text{Fe}_{\text{ppt}}$  data from both replicates resulted in  $\epsilon^{56}\text{Fe}$  of 2.44‰ and 2.98‰, larger than that attained for the  $\delta^{56}\text{Fe}(\text{II})_{\text{aq}}$  data (Table 1) and within the literature range. Prior explanation for the offset in  $\epsilon^{56}\text{Fe}$  between these two fractions is that, following precipitation, the  $\text{Fe}_{\text{ppt}}$  underwent partial equilibration with another phase of iron in the system, possibly a ligand-



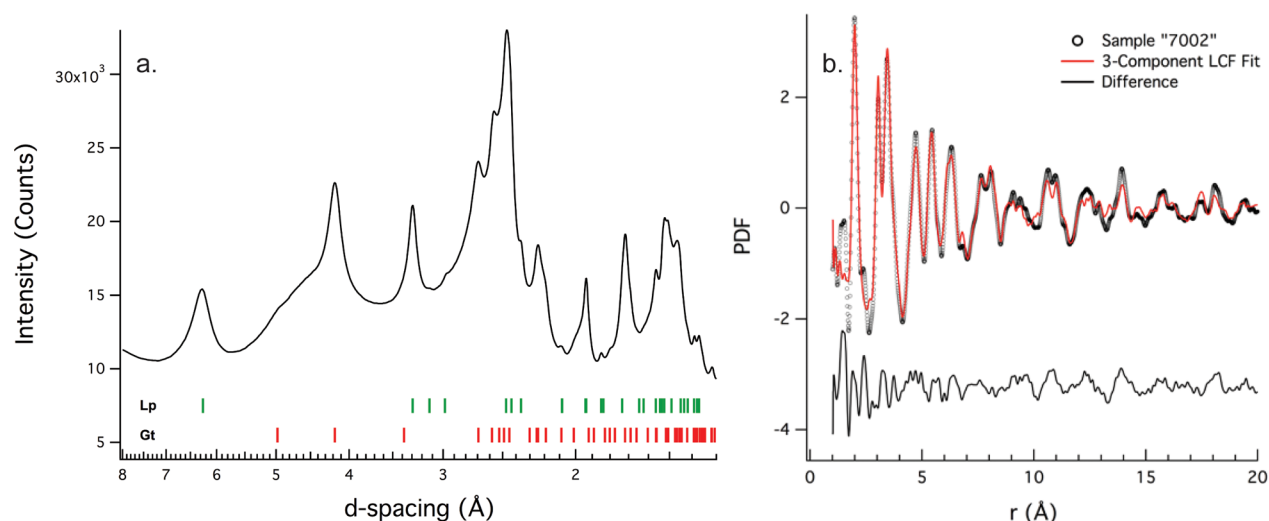


**Figure 2.** (a) X-ray diffraction (XRD) pattern obtained from X-ray total scattering data of the  $\text{Fe}_{\text{ppt}}$  phase after complete  $\text{Fe(II)}$  oxidation, freeze-drying, and water washing. The indexed reflections for lepidocrocite (Lp) and goethite (Gt) are shown. (b) A 3-component linear combination fit of 58% ferrihydrite, 22% goethite, and 20% lepidocrocite (Supplementary Table 4).

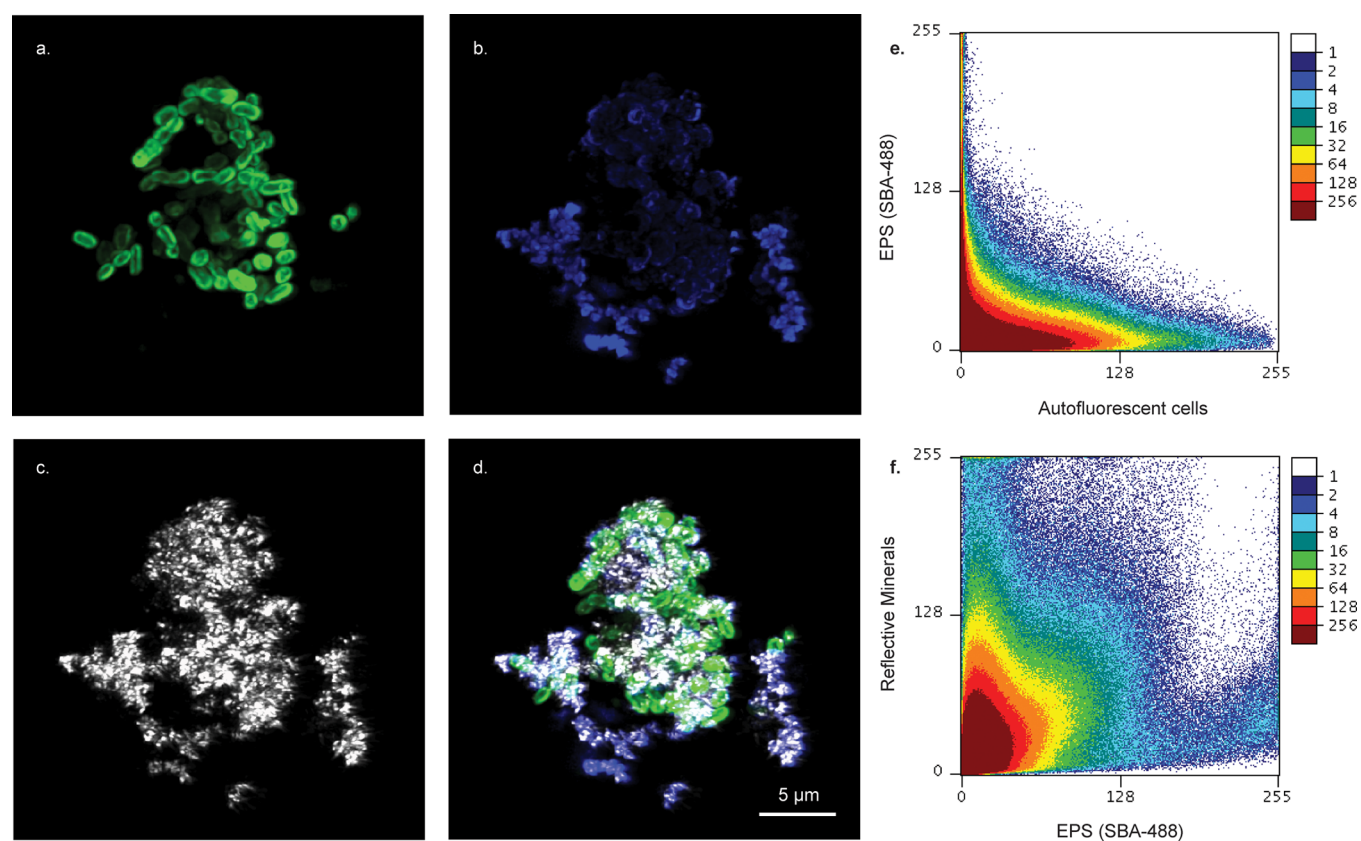


**Figure 3.** CLSM images of *Synechococcus* PCC 7002 cultured anoxically with 4.5 mM  $\text{Fe(II)}$ . (a) Autofluorescent cells, (b) stained with the lectin-binding dye SBA-488, (c) the reflection signal from  $\text{Fe(III)}$  minerals, and (d) an overlay of (a–c). Correlation plot of the fluorescence intensity in individual pixels from (e) autofluorescence (a) vs SBA-488 (b) and (f) SBA-488 (b) vs  $\text{Fe(III)}$  minerals (c). This analysis demonstrates that EPS, which is bound by SBA-488, is coating  $\text{Fe(III)}$  minerals but is not spatially associated with cells.

bound or sorbed  $\text{Fe(III)}$  phase<sup>18,48</sup> or  $\text{Fe(II)}_{\text{aq}}$ .<sup>29,49</sup> Below, we use our mineralogical and microscopic characterizations of the experiment to explore possible exchange processes in this system.

**Iron Sorption to Cells and Minerals.** The third, quantitatively significant fraction of iron in the system in addition to  $\text{Fe(II)}_{\text{aq}}$  and  $\text{Fe}_{\text{ppt}}$  was  $\text{Fe}_{\text{NaAc}}$  (up to 18% of total

$\text{Fe}$ ). The  $\delta^{56}\text{Fe}_{\text{NaAc}}$  data had an intermediate isotopic composition between  $\text{Fe(II)}_{\text{aq}}$  and  $\text{Fe}_{\text{ppt}}$  from 0.10‰ to −0.73‰ throughout the experiment, and contained both  $\text{Fe(II)}$  and  $\text{Fe(III)}$  (Supplementary Table 1). The presence of  $\text{Fe(III)}$  in  $\text{Fe}_{\text{NaAc}}$  has previously been observed in  $\text{Fe(II)}$  oxidation experiments with anoxygenic phototrophs<sup>18</sup> but not with nitrate-dependent  $\text{Fe(II)}$ -oxidizing bacteria.<sup>29</sup> The  $\text{Fe}_{\text{NaAc}}$

must have been sorbed onto one of the surfaces, either  $\text{Fe}_{\text{ppt}}$  or cells, on the basis of its extraction with sodium acetate.<sup>38</sup> In order to infer whether equilibration processes were occurring between  $\text{Fe}_{\text{NaAc}}$  and  $\text{Fe}_{\text{ppt}}$  it is necessary to know (1) where  $\text{Fe}_{\text{NaAc}}$  was in our experiments and (2) what type of iron species [i.e., Fe(II) or Fe(III)] that it was.

Our use of a lectin-binding dye in confocal microscopy documents that EPS was also forming during Fe(II) oxidation with *Synechococcus* PCC 7002 (Figure 3). We can use this data set to first determine whether EPS was important in binding/sorbing iron extracted as  $\text{Fe}_{\text{NaAc}}$  and then to determine whether iron was associated with the surface of cells and/or  $\text{Fe}_{\text{ppt}}$ . An overlay of Figure 3a–c, which show the location of cells, EPS, and  $\text{Fe}_{\text{ppt}}$  indicates that EPS is colocalized with  $\text{Fe}_{\text{ppt}}$  (Figure 3d). The correlation analysis in Figure 3e implies there is no spatial overlap of EPS with cells. In previous work with *Synechococcus* PCC 7002 under identical growth conditions as in Figure 3, a fluorescent sensor for soluble or ligand-bound Fe(III) was used in CLSM, and fluorescence was localized directly at the *Synechococcus* PCC 7002 cell surfaces.<sup>18</sup> While spectral interferences prevented us from simultaneously labeling EPS and Fe(III) in our current CLSM experiments, we can infer from comparing our data set with the previously published one<sup>34</sup> that there was Fe(III) sorbed to the surface of cells but not EPS or  $\text{Fe}_{\text{ppt}}$ .<sup>50</sup> In support of this, EPS is expected to stay with the aqueous phase during filtration through a 0.2  $\mu\text{m}$  filter<sup>51</sup> or be washed off of  $\text{Fe}_{\text{ppt}}$  in the water wash.<sup>18</sup> We did not detect any Fe(III) in the  $\text{Fe(II)}_{\text{aq}}$  fraction or measure any detectable iron in the water wash. From these results, we exclude EPS as having a major role in binding soluble Fe(III) in the current system. This data indicates that cell surfaces sorbed Fe(III). Previous experiments with *Synechococcus* PCC 7002 cells demonstrated that sorption to cells is a major fate for aqueous iron, although the oxidation state of sorbed iron was not determined in those experiments, so we cannot rule out that some Fe(II) was also sorbed to cells.<sup>34</sup> However, sorption onto cells has previously been documented as a fate for aqueous iron with diverse cyanobacteria, with Fe(III) more commonly detected at the cell surface than Fe(II),<sup>22</sup> via attachment of Fe–O–Fe polymers to phosphoryl groups,<sup>22,23</sup> strengthening the inferences made from CLSM that *Synechococcus* PCC 7002 cells sorbed Fe(III).

The other surface in our experiments that could have sorbed iron extracted as  $\text{Fe}_{\text{NaAc}}$  was  $\text{Fe}_{\text{ppt}}$ . The three techniques we used to address mineralogy indicate that our  $\text{Fe}_{\text{ppt}}$  was a mixture of 58% ferrihydrite, 22% goethite, and 20% lepidocrocite (Figure 2), and ferrihydrite was likely the predominant mineral present during the experiments (see Supporting Information). Minerals such as ferrihydrite and goethite, similar to what was present in our experiments, can sorb Fe(II).<sup>27,52</sup> Both Fe(II) and Fe(III) were detected in the  $\text{Fe}_{\text{NaAc}}$  (Supplementary Table 1), raising the possibility that Fe(III) was extracted from the mineral. However, we verified that no Fe(III) was extracted from synthetic ferrihydrite with our 0.5 M sodium acetate solution prior to beginning experiments (data not shown), consistent with previous reports that used a 1 M sodium acetate solution.<sup>38</sup> A further inference in support of sorbed Fe(II) being extracted from  $\text{Fe}_{\text{ppt}}$  by sodium acetate is that  $\text{Fe}_{\text{ppt}}$  still contained some Fe(II) after extraction, as measured by ferrozine (Supplementary Table 1). We take this as evidence that sorbed iron associated with the mineral was predominantly Fe(II), although we cannot exclude

that some Fe(III) may also be sorbed to the mineral surface.<sup>53,54</sup>

**Fractionation Processes.** We observed evidence for three reactions in our experiments that are essential for understanding the observed fractionations of iron isotopes, and these are summarized in Figure 4. They are (1) Fe(II) oxidation to

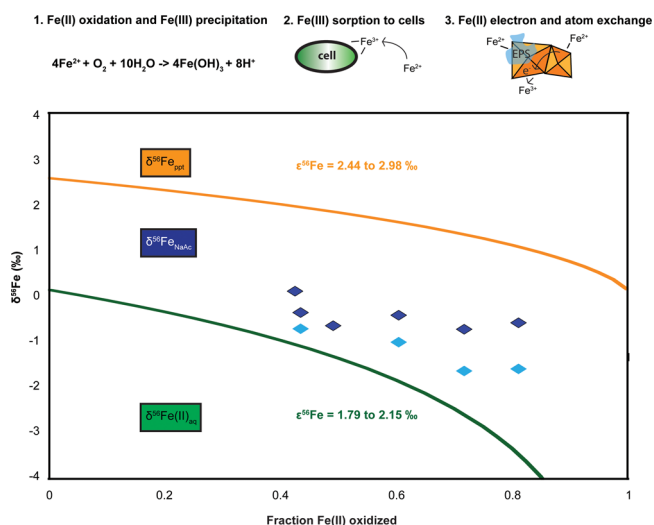


**Figure 4.** Controls on the overall iron isotope fractionation in the system are (1) Fe(II) oxidation and precipitation of Fe(III) as  $\text{Fe}_{\text{ppt}}$ ; (2) sorption of Fe(III) to cells; (3) partial equilibrium atom and electron exchange after sorption of  $\text{Fe(II)}_{\text{aq}}$  to  $\text{Fe}_{\text{ppt}}$ . (1) generates  $\text{Fe}_{\text{ppt}}$  (solid orange line) that is 2–3‰ heavier than  $\text{Fe(II)}_{\text{aq}}$  (solid green line). (2) produces sorbed Fe(III) on cells with an estimated equilibrium  $\Delta^{56}\text{Fe}_{\text{FeNaAc-Fe(II)aq}}$  of 1.84‰.<sup>23</sup> (3) produces Fe(II) sorbed on goethite with an estimated  $\Delta^{56}\text{Fe}_{\text{FeNaAc-Fe(II)aq}}$  of 0.8‰.<sup>54</sup> The resulting  $\delta^{56}\text{Fe}_{\text{NaAc}}$  predicted from (2) and (3) are denoted by the light blue diamonds.

Fe(III), which forms  $\text{Fe}_{\text{ppt}}$  (2) sorption of Fe(III) to cells, and (3) sorption of Fe(II) to  $\text{Fe}_{\text{ppt}}$ . These observations fit a two step-model of Fe(II) oxidation, where Fe(II) is oxidized and undergoes rapid isotopic equilibration with a pool of Fe(III), which then precipitates as Fe(III) minerals.<sup>49</sup> We suggest, however, that in our experiments,  $\text{Fe}_{\text{ppt}}$  undergoes subsequent partial equilibration with  $\text{Fe(II)}_{\text{aq}}$ .

The fitting of our  $\delta^{56}\text{Fe(II)}_{\text{aq}}$  and  $\delta^{56}\text{Fe}_{\text{ppt}}$  with Rayleigh equations representing isolation of the  $\text{Fe}_{\text{ppt}}$  pool from  $\text{Fe(II)}_{\text{aq}}$  after precipitation and a linear equation representing complete isotopic equilibrium are helpful in interpreting the fractionation mechanisms taking place. The larger  $\Sigma\chi^2$  values for linear fits of all data as compared to Rayleigh fits indicate that complete isotopic equilibrium between  $\text{Fe(II)}_{\text{aq}}$  and  $\text{Fe}_{\text{ppt}}$  is not occurring during Fe(II) oxidation and precipitation (Table 1). The smaller  $\epsilon^{56}\text{Fe}$  values for Rayleigh fits of the  $\delta^{56}\text{Fe(II)}_{\text{aq}}$  (1.79‰ and 2.15‰ as compared to 2.44‰ and 2.98‰ for  $\delta^{56}\text{Fe}_{\text{ppt}}$ ) are on the order of fractionation observed in other biological Fe(II) oxidation experiments in batch at circumneutral pH: 1.5‰,<sup>48</sup> 1.5–2‰,<sup>29</sup> and 1–2‰.<sup>18</sup> Such small net fractionations have been noted when the presence of significant quantities of sorbed or ligand-bound Fe(III) has been detected or observed.<sup>29</sup>

Up to a few percent of total iron was found as Fe(III) in the  $\text{Fe}_{\text{NaAc}}$  fraction (Supplementary Table 1). On the basis of detection of iron sorbed to cells with a dye that is specific for an aqueous or ligand-bound Fe(III),<sup>42,43</sup> we suggest that this

Fe(III) could equilibrate with Fe(II)<sub>aq</sub>.<sup>29,48</sup> In experiments with *Synechococcus* sp. cells at pH 6, added Fe(II) [which was adsorbed as Fe(III)] was 1.84‰ heavier than aqueous Fe(II),<sup>23</sup> and equilibrium with Fe(II)<sub>aq</sub> was inferred from the data. This fractionation is very similar to our  $\epsilon^{56}\text{Fe}$  values derived from Rayleigh fits of  $\delta^{56}\text{Fe}(\text{II})_{\text{aq}}$  (1.79‰ and 2.15‰). Because of the similar type of organism that we used, it is likely that equilibrium fractionation between Fe(II)<sub>aq</sub> and Fe(III) sorbed to cells is a relevant process in our experiments.

While the  $\delta^{56}\text{Fe}_{\text{ppt}}$  data are not well fit by a linear model representing complete equilibrium exchange with Fe(II)<sub>aq</sub>, the range of the  $\epsilon^{56}\text{Fe}$  determined from Rayleigh fits of the two  $\delta^{56}\text{Fe}_{\text{ppt}}$  data sets (2.44‰ and 2.98‰) is of the same magnitude expected for equilibrium between Fe<sub>ppt</sub> and Fe(II)<sub>aq</sub>. Wu et al.<sup>31</sup> inferred a  $\Delta^{56}\text{Fe}_{\text{ferrihydrite-Fe(II)aq}}$  (where  $\Delta^{56}\text{Fe}_{\text{ferrihydrite-Fe(II)aq}} = \delta^{56}\text{Fe}_{\text{ferrihydrite}} - \delta^{56}\text{Fe}_{\text{Fe(II)aq}}$ ) of 3.2‰, while Beard et al. and Frierdich et al. reported a  $\Delta^{56}\text{Fe}_{\text{goethite-Fe(II)aq}}$  of 1.1‰.<sup>25,55</sup> Considering the 58% ferrihydrite, 22% goethite, and 20% lepidocrocite in our precipitates as determined from X-ray scattering (Figure 2), the equilibrium  $\Delta^{56}\text{Fe}_{\text{Feppt-Fe(II)aq}}$  for our minerals could range from 2.3‰ to 2.7‰, depending on whether the assumed fractionation for lepidocrocite is the same as for goethite or ferrihydrite, respectively. The larger  $\epsilon^{56}\text{Fe}$  we calculate for our second data set (2.98‰) may reflect that ferrihydrite, with a larger  $\Delta^{56}\text{Fe}$  value, was likely the mineral present during active Fe(II) oxidation (see Supporting Information).

In our batch experiments, Fe(II)<sub>aq</sub> may continue to react with Fe<sub>ppt</sub> given their proximity and the time frame of experiments (10 days). Sorption of Fe(II) on Fe<sub>ppt</sub> provides a likely mechanism for partial isotope equilibrium and is supported by our detection of Fe(II) in Fe<sub>ppt</sub> (Supplementary Table 1). Sorption of Fe(II) is an important pathway in recrystallization of Fe(III) (oxyhydr)oxide minerals, particularly ferrihydrite.<sup>28</sup> During this process, equilibrium atom and electron exchange occur between sorbed Fe(II) and Fe(III) minerals,<sup>24</sup> with complete equilibrium attained within 2 weeks for goethite, for instance<sup>55</sup> (a similar time frame as our 10 day experiment). In this model, Fe(II) sorbs to Fe(III) minerals and donates an electron into the bulk mineral structure, adding to the Fe(III) mineral, and causing the desorption of a newly produced Fe(II) from the mineral. This is also consistent with the shifts in mineralogy we see during the course of oxidation (see Supporting Information).

We do not see evidence for complete equilibrium between Fe(II)<sub>aq</sub> and Fe<sub>ppt</sub> given the poor linear fit of  $\delta^{56}\text{Fe}_{\text{ppt}}$  (Table 1). Atom and electron exchange between Fe<sub>ppt</sub> and sorbed Fe(II) is expected to be diminished in the presence of organic compounds.<sup>30</sup> Our CLSM data indicate that EPS is colocalized to minerals (Figure 2). It is possible that atom and electron exchange can still occur when Fe(III) minerals are coprecipitated with organics, as retardation of this process seems to result from blockage of surface sites when organics coat already formed Fe(III) minerals,<sup>52</sup> or if long chain carbon molecules are present.<sup>30</sup> Therefore, we suggest that only partial atom and electron exchange occurred in our system as a result of the EPS coating the Fe<sub>ppt</sub>.

During atom exchange, the fractionation when Fe(II)<sub>aq</sub> sorbs onto goethite varies among experiments. One study reports sorbed Fe(II) is 0.73‰ heavier than Fe(II)<sub>aq</sub><sup>56</sup> and another reported sorbed Fe(II) was 1.24‰ heavier.<sup>25</sup> Differences are likely due to a lack of equilibrium obtained. Crosby et al.<sup>53,54</sup> directly measured sorbed Fe(II) extracted with sodium acetate

during microbial Fe(III) reduction experiments, which was just 0.3‰ heavier than Fe(II)<sub>aq</sub> for experiments using hematite and up to 0.8‰ heavier for experiments using goethite as the sorbing surface. Our  $\Delta^{56}\text{Fe}_{\text{FeNaAc-Fe(II)aq}}$  ranged from 0.45‰ to 2.66‰, which is much larger and more variable than the experiments of Crosby et al.,<sup>53,54</sup> which may be in part because our Fe<sub>NaAc</sub> includes both Fe(II) and Fe(III). Another factor is that, in our experiments, the less crystalline mineral ferrihydrite was likely the sorbing surface present during experiments (see Supplementary Figures 1 and 2 and Supporting Information). Several studies have noted a trend of larger fractionations during sorption to less crystalline minerals or higher surface area minerals.<sup>25,54</sup> The Fe<sub>ppt</sub> in our experiments had a surface area of 122.1 m<sup>2</sup> g<sup>-1</sup>.

We calculated  $\delta^{56}\text{Fe}_{\text{NaAc}}$  considering that the Fe(III) fraction of Fe<sub>NaAc</sub> should be 1.84‰ heavier than Fe(II)<sub>aq</sub> due to adsorption of Fe(III) at cell surfaces,<sup>23</sup> and the sorbed Fe(II) fraction of Fe<sub>NaAc</sub> should be at least 0.8‰ heavier than Fe(II)<sub>aq</sub>. The calculated  $\delta^{56}\text{Fe}_{\text{NaAc}}$  is a good model of our actual  $\delta^{56}\text{Fe}_{\text{NaAc}}$  values (Figure 4). This calculation supports the model presented here, in which Fe(II) is oxidized to Fe(III), which is sorbed onto cells and equilibrates with Fe(II)<sub>aq</sub>, and full equilibration of Fe(II)<sub>aq</sub> with Fe<sub>ppt</sub> via atom and electron exchange is hindered by the presence of EPS on Fe<sub>ppt</sub>.

Our experiments provide evidence that iron isotope fractionation during microbially influenced Fe(II) oxidation by cyanobacteria is not a simple reaction, controlled only by the abiotic oxidation of Fe(II) with oxygen and rapid precipitation of Fe(III) at circumneutral pH.<sup>34</sup> Multiple secondary processes generate a significant fraction of sorbed iron that is isotopically distinct from either residual Fe(II)<sub>aq</sub> or Fe<sub>ppt</sub>, and subsequent equilibration between the iron pools can further modify the isotopic composition of these phases. Our data indicate that sorption of Fe(III) at cell surfaces likely further fractionates the Fe(II)<sub>aq</sub> pool. In addition, abiotic sorption of Fe(II) to Fe(III) mineral surfaces can also fractionate Fe(II)<sub>aq</sub>, through equilibrium atom and electron exchange subsequent to Fe(II) sorption, despite the presence of EPS. Follow-up experiments could investigate atom and electron exchange in this system. Specifically, isotopically enriched Fe(II)<sub>aq</sub> solutions mixed with preformed cells and minerals would be useful for monitoring atom exchange between the Fe(II)<sub>aq</sub> and Fe<sub>ppt</sub>.<sup>57</sup>

The processes and phases described here can overprint the anticipated fractionations and compositions of Fe(III) minerals and organic-associated iron present in the environment and can challenge interpretation of the genesis of Fe(III) minerals in the geological record, where the residual Fe(II)<sub>aq</sub> pool is no longer present.<sup>12,58–60</sup> Although iron atom and electron exchange has received the most attention as a process relevant to Fe(III)-reducing systems where Fe(II) is in contact with Fe(III) minerals, our data suggest this process could also be relevant in environments where Fe(II) is abundant during Fe(II) oxidation and Fe(III) mineral formation. This includes oxidizing environments with high enough fluxes of Fe(II) for Fe(II) to persist even in the face of rapid oxidation,<sup>2,61</sup> such as Fe(II)-rich springs or seeps and marine upwelling zones that tap ferruginous bottom waters, past or present.<sup>33</sup> Furthermore, our work documents atom and electron exchange in the presence of iron minerals whose formation pathways are biologically induced and when organic phases coat iron minerals. Finally, iron redox cycling and sorption of iron at the surface of cyanobacteria may be an important component of modern and



ancient aquatic iron cycling, and our work highlights the effect of such processes on iron isotope systematics.

## ■ ASSOCIATED CONTENT

### Supporting Information

The Supporting Information is available free of charge on the ACS Publications website at DOI: 10.1021/acs.est.6b05833.

Supporting methods, discussion, additional spectra, and tables of Fe(II) and Fe(total) concentrations, <sup>57</sup>Fe Mössbauer fitting parameters, *k*<sup>3</sup>-weighted Fe K-edge fit results, and linear combination fit (PDF)

## ■ AUTHOR INFORMATION

### Corresponding Author

\*Phone: (515) 294-5826; fax: (515) 294-6049; e-mail: [eswanner@iastate.edu](mailto:eswanner@iastate.edu).

### ORCID

E. D. Swanner: 0000-0001-9507-0893

A. Kappler: 0000-0002-3558-9500

### Present Address

#State Key Laboratory of Environmental Geochemistry Institute of Geochemistry, Chinese Academy of Sciences Lincheng West Road 99, Guiyang 550081, P. R. China

### Notes

The authors declare no competing financial interest.

## ■ ACKNOWLEDGMENTS

*Synechococcus* PCC 7002 was a gift of M. Eisenhut. E. Reitter assisted with iron purification and isotope analysis. E. Struve performed the Mastersizer and BET analyses. Portions of this research were carried out at the Stanford Synchrotron Radiation Lightsource (SSRL), a directorate of SLAC National Accelerator Laboratory and an Office of Science User Facility operated by the U.S. Department of Energy Office of Science by Stanford University. R. Davis assisted with EXAFS measurements. The use of the Advanced Photon Source, an Office of Science User Facility operated for the U.S. Department of Energy (DOE) Office of Science by Argonne National Laboratory, was supported by the U.S. DOE under Contract No. DE-AC02-06CH11357. We thank K. Chapman, P. Chupas, and K. Beyer for their support at APS beamline 11-ID-B. E.D.S. was supported by a Carl Zeiss Stiftung Postdoctoral Fellowship, which also supported the work of T.B.W.W. received support from Sino-German (CSC-DAAD) Postdoc Scholarship Program and China Postdoctoral Science Foundation (2014M560115). F.M.M. received support from the Center for Environmental Implications of Nanotechnology (CEINT) funded under NSF cooperative agreement EF-0830093. A.K. was supported by the German Research Foundation (DFG, KA 1736/24-1) and by the European Research Council under the European Union's Seventh Framework Programme (FP/2007–2013)/ERC Grant, Agreement no. 307320 – MICROFOX.

## ■ REFERENCES

(1) Melton, E. D.; Swanner, E. D.; Behrens, S.; Schmidt, C.; Kappler, A. The interplay of microbially mediated and abiotic reactions in the biogeochemical Fe cycle. *Nat. Rev. Microbiol.* **2014**, *12*, 797–808.  
 (2) Trouwborst, R. E.; Johnston, A.; Koch, G.; Luther, G. W., III; Pierson, B. K. Biogeochemistry of Fe(II) oxidation in a photosynthetic microbial mat: Implications for Precambrian Fe(II) oxidation. *Geochim. Cosmochim. Acta* **2007**, *71*, 4629–4643.

(3) Epping, E. H. G.; Schoemann, V.; de Heij, H. Manganese and Iron Oxidation During Benthic Oxygenic Photosynthesis. *Estuarine, Coastal Shelf Sci.* **1998**, *47* (6), 753–767.

(4) Conway, T. M.; John, S. G. Quantification of dissolved iron sources to the North Atlantic Ocean. *Nature* **2014**, *511* (7508), 212–215.

(5) Scholz, F.; McManus, J.; Mix, A. C.; Hensen, C.; Schneider, R. R. The impact of ocean deoxygenation on iron release from continental margin sediments. *Nat. Geosci.* **2014**, *7* (6), 433–437.

(6) Staubwasser, M.; von Blanckenburg, F.; Schoenberg, R. Iron isotopes in the early marine diagenetic iron cycle. *Geology* **2006**, *34* (8), 629–632.

(7) Severmann, S.; Lyons, T. W.; Anbar, A.; McManus, J.; Gordon, G. Modern iron isotope perspective on the benthic iron shuttle and the redox evolution of ancient oceans. *Geology* **2008**, *36* (6), 487–490.

(8) Stramma, L.; Johnson, G. C.; Sprintall, J.; Mohrholz, V. Expanding Oxygen-Minimum Zones in the Tropical Oceans. *Science* **2008**, *320* (5876), 655–658.

(9) Poulton, S. W.; Canfield, D. E. Ferruginous Conditions: A Dominant Feature of the Ocean through Earth's History. *Elements* **2011**, *7* (2), 107–112.

(10) Canfield, D. E.; Poulton, S. W.; Narbonne, G. M. Late-Neoproterozoic deep-ocean oxygenation and the rise of animal life. *Science* **2007**, *315*, 92–95.

(11) Scott, C.; Lyons, T. W.; Bekker, A.; Shen, Y.; Poulton, S. W.; Chu, X.; Anbar, A. D. Tracing the stepwise oxygenation of the Proterozoic ocean. *Nature* **2008**, *452* (27), 456–459.

(12) Czaja, A. D.; Johnson, C. M.; Roden, E. E.; Beard, B. L.; Vogelin, A. R.; Nägler, T. F.; Beukes, N. J.; Wille, M. Evidence for free oxygen in the Neoproterozoic ocean based on coupled iron-molybdenum isotope fractionation. *Geochim. Cosmochim. Acta* **2012**, *86*, 118–137.

(13) Sahoo, S. K.; Planavsky, N. J.; Kendall, B.; Wang, X.; Shi, X.; Scott, C.; Anbar, A. D.; Lyons, T. W.; Jiang, G. Ocean oxygenation in the wake of the Marinoan glaciation. *Nature* **2012**, *489* (7417), 546–549.

(14) Beard, B. L.; Johnson, C. M.; Cox, L.; Sun, H.; Nealson, K.; Aguilar, C. Iron Isotope Biosignatures. *Science* **1999**, *285*, 1889–1892.

(15) Johnson, C. M.; Beard, B. L.; Roden, E. E. The Iron Isotope Fingerprints of Redox and Biogeochemical Cycling in Modern and Ancient Earth. *Annu. Rev. Earth Planet. Sci.* **2008**, *36* (1), 457–493.

(16) Schauble, E. A. Applying Stable Isotope Fractionation Theory to New Systems. *Rev. Mineral. Geochem.* **2004**, *55* (1), 65–111.

(17) Balci, N.; Bullen, T. D.; Witte-Lien, K.; Shanks, W. C.; Motelica, M.; Mandernack, K. W. Iron isotope fractionation during microbially stimulated Fe(II) oxidation and Fe(III) precipitation. *Geochim. Cosmochim. Acta* **2006**, *70*, 622–639.

(18) Swanner, E. D.; Wu, W.; Schoenberg, R.; Byrne, J.; Michel, F. M.; Pan, Y.; Kappler, A. Fractionation of Fe isotopes during Fe(II) oxidation by a marine photoferrotroph is controlled by the formation of organic Fe-complexes and colloidal Fe fractions. *Geochim. Cosmochim. Acta* **2015**, *165* (0), 44–61.

(19) Kranzler, C.; Lis, H.; Shaked, Y.; Keren, N. The role of reduction in iron uptake processes in a unicellular, planktonic cyanobacterium. *Environ. Microbiol.* **2011**, *13* (11), 2990–9.

(20) Lis, H.; Kranzler, C.; Keren, N.; Shaked, Y. A Comparative Study of Iron Uptake Rates and Mechanisms amongst Marine and Fresh Water Cyanobacteria: Prevalence of Reductive Iron Uptake. *Life* **2015**, *5* (1), 841–860.

(21) Rose, A. L.; Salmon, T. P.; Lukondeh, T.; Neilan, B. A.; Waite, T. D. Use of superoxide as an Electron Shuttle for Iron Acquisition by the Marine Cyanobacterium *Lyngbya majuscula*. *Environ. Sci. Technol.* **2005**, *39*, 3708–3715.

(22) González, A. G.; Pokrovsky, O. S.; Jiménez-Villacorta, F.; Shirokova, L. S.; Santana-Casiano, J. M.; González-Dávila, M.; Emnova, E. E. Iron adsorption onto soil and aquatic bacteria: XAS structural study. *Chem. Geol.* **2014**, *372* (0), 32–45.

(23) Mulholland, D. S.; Poitrasson, F.; Shirokova, L. S.; González, A. G.; Pokrovsky, O. S.; Boaventura, G. R.; Vieira, L. C. Iron isotope



fractionation during Fe(II) and Fe(III) adsorption on cyanobacteria. *Chem. Geol.* **2015**, *400* (0), 24–33.

(24) Williams, A. G. B.; Scherer, M. M. Spectroscopic Evidence for Fe(II)-Fe(III) Electron Transfer at the Iron Oxide-Water Interface. *Environ. Sci. Technol.* **2004**, *38*, 4782–4790.

(25) Beard, B. L.; Handler, R. M.; Scherer, M. M.; Wu, L.; Czaja, A. D.; Heimann, A.; Johnson, C. M. Iron isotope fractionation between aqueous ferrous iron and goethite. *Earth Planet. Sci. Lett.* **2010**, *295* (1–2), 241–250.

(26) Johnson, C. M.; Roden, E. E.; Welch, S. A.; Beard, B. L. Experimental constraints on Fe isotope fractionation during magnetite and Fe carbonate formation coupled to dissimilatory hydrous ferric oxide reduction. *Geochim. Cosmochim. Acta* **2005**, *69* (4), 963–993.

(27) Hansel, C. M.; Benner, S. G.; Neiss, J.; Dohnalkova, A.; Kukkadapu, R. K.; Fendorf, S. Secondary mineralization pathways induced by dissimilatory iron reduction of ferrihydrite under advective flow. *Geochim. Cosmochim. Acta* **2003**, *67* (16), 2977–2992.

(28) Hansel, C. M.; Benner, S. G.; Nico, P.; Fendorf, S. Structural constraints of ferric (hydr)oxides on dissimilatory iron reduction and the fate of Fe(II). *Geochim. Cosmochim. Acta* **2004**, *68* (15), 3217–3229.

(29) Kappler, A.; Johnson, C. M.; Crosby, H. A.; Beard, B. L.; Newman, D. K. Evidence for equilibrium iron isotope fractionation by nitrate-reducing iron(II)-oxidizing bacteria. *Geochim. Cosmochim. Acta* **2010**, *74* (10), 2826–2842.

(30) Pasakarnis, T.; McCormick, M. L.; Parkin, G. F.; Thompson, A.; Scherer, M. FeIIaq-FeIIIoxide electron transfer and Fe exchange - effect of organic carbon. *Environ. Chem.* **2015**, *12*, 52–63.

(31) Wu, L.; Beard, B. L.; Roden, E. E.; Johnson, C. M. Stable Iron Isotope Fractionation Between Aqueous Fe(II) and Hydrous Ferric Oxide. *Environ. Sci. Technol.* **2011**, *45*, 1847–1852.

(32) Reddy, T. R.; Frierdich, A. J.; Beard, B. L.; Johnson, C. M. The effect of pH on stable iron isotope exchange and fractionation between aqueous Fe(II) and goethite. *Chem. Geol.* **2015**, *397*, 118–127.

(33) Swanner, E. D.; Młoszewska, A. M.; Cirpka, O. A.; Schoenberg, R.; Konhauser, K. O.; Kappler, A. Modulation of oxygen production in Archaean oceans by episodes of Fe(II) toxicity. *Nat. Geosci.* **2015**, *8* (2), 126–130.

(34) Swanner, E. D.; Wu, W.; Hao, L.; Wuestner, M.; Obst, M.; Moran, D. M.; McIlvin, M.; Saito, M.; Kappler, A. Physiology, Fe(II) oxidation, and Fe mineral formation by a marine planktonic cyanobacterium grown under ferruginous conditions. *Front. Earth Sci.* **2015**, *3*; DOI: 10.3389/feart.2015.00060.

(35) Wu, W.; Swanner, E. D.; Hao, L.; Zeitvogel, F.; Obst, M.; Pan, Y.; Kappler, A. Characterization of the physiology and cell-mineral interactions of the marine anoxygenic phototrophic Fe(II)-oxidizer *Rhodovulum iodotum* - implications for Precambrian Fe(II) oxidation. *FEMS Microbiol. Ecol.* **2014**, *88*, 503–515.

(36) Llíros, M.; García-Armisen, T.; Darchambeau, F.; Morana, C.; Triadó-Margarit, X.; Inceoğlu, Ö.; Borrego, C. M.; Bouillon, S.; Servais, P.; Borges, A. V.; Descy, J. P.; Canfield, D. E.; Crowe, S. A. Pelagic photoferrotrophy and iron cycling in a modern ferruginous basin. *Sci. Rep.* **2015**, *5*, 13803.

(37) Busigny, V.; Planavsky, N. J.; Jézéquel, D.; Crowe, S.; Louvat, P.; Moureaux, J.; Viollier, E.; Lyons, T. W. Iron isotopes in an Archean ocean analogue. *Geochim. Cosmochim. Acta* **2014**, *133*, 443–462.

(38) Crosby, H.; Johnson, C.; Roden, E.; Beard, B. Coupled Fe(II)-Fe(III) electron and atom exchange as a mechanism for Fe Isotope fractionation during dissimilatory iron oxide reduction. *Environ. Sci. Technol.* **2005**, *39*, 6698–6704.

(39) Stookey, L. L. Ferrozine - a new spectrophotometric reagent for iron. *Anal. Chem.* **1970**, *42* (7), 779–781.

(40) Schoenberg, R.; Von Blanckenburg, F. An assessment of the accuracy of stable Fe isotope ratio measurements on samples with organic and inorganic matrices by high-resolution multicollector ICP-MS. *Int. J. Mass Spectrom.* **2005**, *242*, 257–272.

(41) Moeller, K.; Schoenberg, R.; Grenne, T.; Thorseth, I. H.; Drost, K.; Pedersen, R. B. Comparison of iron isotope variations in modern

and Ordovician siliceous Fe oxyhydroxide deposits. *Geochim. Cosmochim. Acta* **2014**, *126* (0), 422–440.

(42) Mao, J.; He, Q.; Liu, W. An rhodamine-based fluorescence probe for iron(III) ion determination in aqueous solution. *Talanta* **2010**, *80* (5), 2093–2098.

(43) Mao, J.; Wang, L.; Dou, W.; Tang, X.; Yan, Y.; Liu, W. Tuning the Selectivity of Two Chemosensors to Fe(III) and Cr(III). *Org. Lett.* **2007**, *9* (22), 4567–4570.

(44) Schmid, G.; Zeitvogel, F.; Hao, L.; Ingino, P.; Floetenmeyer, M.; Stierhof, Y.-D.; Schroepel, B.; Burkhardt, C.; Kappler, A.; Obst, M. 3D analysis of bacterial cell-(iron)mineral aggregates formed during Fe(II) oxidation by the nitrate-reducing *Acidovorax* sp. strain BoFeN1 using complementary microscopy tomography approaches. *Geobiology* **2014**, *12*, 340–361.

(45) Zeitvogel, F.; Schmid, G.; Hao, L.; Ingino, P.; Obst, M. ScatterJ: an ImageJ plugin for the evaluation of analytical microscopy datasets. *J. Microsc.* **2016**, *261*, 148–156.

(46) Abràmoff, M. D.; Magalhães, P. J.; Ram, S. J. Image processing with IMAGEJ. *Biophotonics Int.* **2004**, *11*, 36–42.

(47) Stumm, W.; Lee, G. F. Oxygenation of Ferrous Iron. *Ind. Eng. Chem.* **1961**, *53*, 143–146.

(48) Croal, L. R.; Johnson, C. M.; Beard, B. L.; Newman, D. K. Iron isotope fractionation by Fe(II)-oxidizing photoautotrophic bacteria. *Geochim. Cosmochim. Acta* **2004**, *68* (6), 1227–1242.

(49) Beard, B.; Johnson, C. M. Fe Isotope Variations in the Modern and Ancient Earth and Other Planetary Bodies. *Rev. Mineral. Geochem.* **2004**, *55*, 319–357.

(50) Hao, L.; Guo, Y.; Byrne, J. M.; Zeitvogel, F.; Schmid, G.; Ingino, P.; Li, J.; Neu, T. R.; Swanner, E. D.; Kappler, A.; Obst, M. Binding of heavy metal ions in aggregates of microbial cells, EPS and biogenic iron minerals measured in-situ using metal- and glycoconjugate-specific fluorophores. *Geochim. Cosmochim. Acta* **2016**, *180*, 66–96.

(51) Bramhachari, P. V.; Dubey, S. K. Isolation and characterization of exopolysaccharide produced by *Vibrio harveyi* strain VB23. *Lett. Appl. Microbiol.* **2006**, *43* (5), 571–577.

(52) Jones, A. M.; Collins, R. N.; Rose, J.; Waite, T. D. The effect of silica and natural organic matter on the Fe(II)-catalysed transformation and reactivity of Fe(III) minerals. *Geochim. Cosmochim. Acta* **2009**, *73* (15), 4409–4422.

(53) Crosby, H. A.; Johnson, C. M.; Roden, E. E.; Beard, B. L. Coupled Fe(II)-Fe(III) Electron and Atom Exchange as a Mechanism for Fe Isotope Fractionation during Dissimilatory Iron Oxide Reduction. *Environ. Sci. Technol.* **2005**, *39* (17), 6698–6704.

(54) Crosby, H. A.; Roden, E. E.; Johnson, C. M.; Beard, B. L. The mechanisms of iron isotope fractionation produced during dissimilatory Fe (III) reduction by *Shewanella putrefaciens* and *Geobacter sulfurreducens*. *Geobiology* **2007**, *5*, 169–189.

(55) Frierdich, A. J.; Beard, B. L.; Reddy, T. R.; Scherer, M. M.; Johnson, C. M. Iron isotope fractionation between aqueous Fe(II) and goethite revisited: New insights based on a multi-direction approach to equilibrium and isotopic exchange rate modification. *Geochim. Cosmochim. Acta* **2014**, *139*, 383–398.

(56) Mikutta, C.; Wiederhold, J. G.; Cirpka, O. A.; Hofstetter, T. B.; Bourdon, B.; Von Gunten, U. Iron isotope fractionation and atom exchange during sorption of ferrous iron to mineral surfaces. *Geochim. Cosmochim. Acta* **2009**, *73*, 1795–1812.

(57) Welch, S. A.; Beard, B. L.; Johnson, C. M.; Braterman, P. S. Kinetic and equilibrium Fe isotope fractionation between aqueous Fe(II) and Fe(III). *Geochim. Cosmochim. Acta* **2003**, *67* (22), 4231–4250.

(58) Planavsky, N.; Rouxel, O. J.; Bekker, A.; Hofmann, A.; Little, C. T. S.; Lyons, T. W. Iron isotope composition of some Archean and Proterozoic iron formations. *Geochim. Cosmochim. Acta* **2012**, *80* (0), 158–169.

(59) Johnson, C. M.; Beard, B. L.; Klein, C.; Beukes, N. J.; Roden, E. E. Iron isotopes constrain biologic and abiologic processes in banded iron formation genesis. *Geochim. Cosmochim. Acta* **2008**, *72* (1), 151–169.

(60) Rouxel, O. J.; Bekker, A.; Edwards, K. J. Iron Isotope Constraints on the Archean and Paleoproterozoic Ocean Redox State. *Science* **2005**, *307* (5712), 1088–1091.

(61) Wu, L.; Brucker, R. P.; Beard, B. L.; Roden, E. E.; Johnson, C. M. Iron isotope characteristics of hot springs at Chocolate Pots, Yellowstone National Park. *Astrobiology* **2013**, *13* (11), 1091–1101.